

***Ab initio* calculation of the structural and electronic properties of carbon and boron nitride using ultrasoft pseudopotentials**

J. Furthmüller, J. Hafner, and G. Kresse

Institut für Theoretische Physik, TU Wien, Wiedner Hauptstraße 8 - 10, A-1040 Wien, Austria

(Received 22 June 1994)

We present *ab initio* calculations of the structural, cohesive, and electronic properties of various polymorphic forms of carbon and boron nitride. Our calculations are based on ultrasoft pseudopotentials and a variational approach to the solution of the Kohn-Sham equations. Optimization of the atomic geometries is performed using total energy calculations and by minimizing the energy via a quasi-Newton quench using the Hellmann-Feynman forces. Special attention is devoted to the convergence of the results with respect to the plane-wave basis. The entire set of structural energy differences calculated in our work is in good agreement with the most accurate results obtained using a variety of different techniques—our results represent a consistent set of data based all on the same potential. We show that the use of ultrasoft potentials allows one to achieve accurate results with low cutoff energies (and hence small basis sets).

I. INTRODUCTION

In recent years, the physical and chemical properties of carbon and boron nitride have been studied in great detail, both theoretically and experimentally. This is mainly due to the fascinating properties of the cubic phases of these materials, such as extreme hardness, high melting point, low dielectric constant, large band gap, etc., that have many applications in modern microelectronic devices and as a protective coating material.^{1,2} Both C and BN occur in different crystallographic forms with strikingly different physical properties. The natural forms of C are graphite (occurring in a hexagonal structure intermixed with 5–15% of a rhombohedral stacking variant⁴) and diamond. Diamond is known in its natural cubic crystal structure⁵ and in a hexagonal form which may be synthesized from graphite.⁶ Possible phase transitions at very high pressures (in analogy with the high-pressure behavior of the other group-IV semiconductors) have been discussed.^{7,8} BN exhibits solid phases similar to those of carbon. Normally BN is found in the hexagonal (graphitelike) phase⁹ with a two-layer stacking sequence, but a rhombohedral form with a three-layer stacking also exists. The denser zinc-blende and wurtzite forms are similar to cubic and hexagonal diamond and may be synthesized under static and dynamic compression.^{10,11} Amorphous forms of both C and BN may be prepared by chemical vapor deposition or sputter deposition, the physical and chemical properties depending strongly upon the conditions under which the thin films have been prepared.^{12–16}

From the theoretical side, the structure and phase stability of materials may be investigated using total-energy and electronic-structure calculations based on the local-density approximation (LDA) to density-functional theory.¹⁷ One of the most popular methods uses the pseudopotential approximation and plane-wave basis sets.^{18,19} In recent years, this technique has gained par-

ticular importance because, with the development of the Car-Parrinello molecular dynamics schemes²⁰ and of efficient conjugate-gradient techniques,^{21,22} it has become possible to study very large systems suitable for studying surfaces, interfaces, and defects in crystalline materials and amorphous materials. However, even with modern computer performance, the application of this technique to materials such as the transition metals or first-row elements is still difficult due to the enormous number of plane waves needed to represent the sharply peaked valence states arising from the strongly attractive electron-ion pseudopotentials. For this reason, total-energy methods working in an augmented-plane-wave or local-orbital basis are of particular importance for these materials.

The structural phase-stability of carbon has been studied using pseudopotentials in a plane-wave^{7,8,23–26} or local-orbital basis,^{27,28} using the linear muffin-tin orbital²⁹ (LMTO) and full-potential linear augmented-plane-wave³⁰ (FLAPW) techniques. The results obtained using the various techniques lead to a rather consistent picture of the cohesive properties of the graphitic and diamondlike phases, and for the phase transitions occurring under very high pressure, although the results have been obtained using different potentials and basis sets. A completely consistent set of structural energy differences (calculated all using the same technique) does not exist as yet. The difficult point remains to determine the extremely small structural energy difference between hexagonal graphite and cubic diamond. The calculations predict the cohesive energy of graphite to be slightly smaller (by 0.009 eV/atom) than that of diamond²⁷ so that the observed stability of graphite would be attributable to a lower vibrational free energy, even in the low-temperature limit (the difference in the zero-point vibrational energies²⁷ calculated from the experimental phonon densities of states^{31,32} is -0.01 eV/atom). It is true that these extremely small energy differences eventually exceed the accuracy of the calculations.

The situation for boron nitride is more complex. Calculations of the structural and cohesive properties of the various polymorphs have been performed using pseudopotentials and plane waves,^{33,34} pseudopotentials (PP's) and a localized basis,³⁵ the FLAPW method,^{36,37} and a tight-binding (TB) technique.³⁸ Whereas the PP calculation³⁵ predicts a lower energy for the cubic phase (by 0.12 eV/atom pair) so that the observed phase stability of the graphitelike phase would again be attributable to differences in the zero-point energies, the TB calculation³⁸ predicts that the total electronic energy of the hexagonal phase is lower by as much as 0.70 eV/atom pair.

In the present paper we return to this problem. We present extensive investigations of the phase stability of carbon and boron nitride, based on a pseudopotential with optimized plane-wave convergence. In Sec. II we review very briefly the construction of the "ultrasoft" pseudopotentials and the formalism for calculating total energies, forces on atoms, and stresses. Sections III and IV describe our results for the structural and electronic properties of C and BN, respectively. In Sec. V we present our conclusions.

II. ULTRASOFT PSEUDOPOTENTIALS

Attempts to solve the convergence problems that arise in the application of pseudopotentials with plane-wave (PW) basis sets to transition metals and first-row elements have been made on two different levels:

(i) It is now generally agreed that it is most convenient to construct the pseudo-wave-functions directly. For a continuous pseudopotential, the pseudo-wave-functions Φ_i^{ps} must be at least two times continuously differentiable at the cutoff radius R_c ; i.e., the ansatz for Φ_i^{ps} must contain a minimum number of four adjustable parameters if in addition the conservation of the norm of Φ_i^{ps} is required.^{39,40} Additional parameters are introduced with the aim to improve the convergence of an expansion of Φ_i^{ps} in a basis of plane waves.⁴¹⁻⁴⁵ A very different scheme for optimizing normconserving pseudopotentials has been introduced by Rabe, Rappe, Kaxiras, and Joannopoulos (RRKJ),⁴³ based on the observation that the convergence of the total energy of a solid with the cutoff energy of the basis set mirrors the convergence of the total energy of an isolated pseudoatom and that total-energy convergence and kinetic-energy convergence are similar in the limit of high cutoff energies. Very recently, the RRKJ scheme was reexamined by Lin *et al.*⁴⁶ and Kresse and Hafner⁴⁷ and it was shown that the minimal form of the RRKJ ansatz, representing Φ_i^{ps} for $r \leq R_c$ in the form of a linear combination of three spherical Bessel functions $j_l(q_i r)$ [with the q_i 's chosen such that the logarithmic derivative of $j_l(q_i r)$ joins smoothly to the logarithmic derivative of the all-electron orbital Ψ_i^{AE} at R_c and that there are $(i-1)$ nodes within $r < R_c$] already optimizes the PW convergence of the pseudopotential for a given cutoff radius R_c . Increasing R_c helps to reduce the cutoff energy E_{cut} , but reduces the transferability

and accuracy of the pseudopotential.

(ii) Vanderbilt^{48,49} pointed out that the main obstacle to a further increase of R_c (and hence a reduction of E_{cut}) is the requirement of norm conservation, forcing the pseudo-wave-function to reproduce the sharp peak of the all-electron wave function. Dropping the norm-conservation constraint, however, makes the logarithmic derivative of Φ_i^{ps} deviate rather quickly from its all-electron value as the energy moves away from the reference energy. Vanderbilt proposed to improve the logarithmic derivative by fitting not just one, but at least two different reference energies and to use a small set of localized functions ("augmentation functions") to describe the charge-density deficit created by the violation of the norm. It has been shown that the new ultrasoft pseudopotentials with large cutoff radii and low cutoff energies are as accurate as norm-conserving pseudopotentials.

A. Construction of ultrasoft pseudopotentials

The all-electron eigenvalues ϵ_n and wave functions $|\Psi_n\rangle$ of the atomic reference state are defined by the Schrödinger equation (in the following we use the notation Ψ for all-electron wave functions and Φ for pseudo-wave-functions; n is a shorthand notation for a set of quantum numbers)

$$(T + V^{\text{AE}} - \epsilon)|\Psi_n\rangle = 0 . \quad (1)$$

For the construction of the ultrasoft pseudopotential we define the following quantities⁴⁷⁻⁵⁴ (V_{loc} is the local part of the pseudopotential which may, in principle, be chosen arbitrarily):

$$|\chi_n\rangle = (\epsilon - T - V^{\text{loc}})|\Phi_n\rangle , \quad (2)$$

$$B_{nm} = \langle \Phi_m | \chi_n \rangle , \quad (3)$$

$$|\beta_n\rangle = \sum_m (B^{-1})_{nm} |\chi_m\rangle , \quad (4)$$

$$Q_{nm}(\mathbf{r}) = \Psi_m^*(\mathbf{r})\Psi_n(\mathbf{r}) - \Phi_m^*(\mathbf{r})\Phi_n(\mathbf{r}) , \quad (5)$$

$$\begin{aligned} q_{nm} &= \langle \Psi_m | \Psi_n \rangle_{R_c} - \langle \Phi_m | \Phi_n \rangle_{R_c} \\ &= \int_{|\mathbf{r}| < R_c} Q_{nm}(\mathbf{r}) d^3r , \end{aligned} \quad (6)$$

$$D_{nm} = B_{nm} + \epsilon Q_{nm} , \quad (7)$$

$$S = 1 + \sum_{nm} Q_{nm} |\beta_m\rangle \langle \beta_n| . \quad (8)$$

It can be shown that the pseudo-wave-functions satisfy the generalized eigenvalue relation

$$\left(T + V_{\text{loc}} + \sum_{nm} D_{nm} |\beta_m\rangle \langle \beta_n| \right) |\Phi_i\rangle = \epsilon_i S |\Phi_i\rangle, \quad (9)$$

with the overlap matrix S defined in (8) and the nonlocal pseudopotential

$$V_{\text{NL}} = \sum_{n,m} D_{nm} |\beta_m\rangle \langle \beta_n|. \quad (10)$$

The total valence charge density $n(\mathbf{r})$ is given as the sum of a smooth part described in terms of the pseudo-wave-functions $|\Phi_i\rangle$ and a localized part described in terms of the augmentation function $Q_{nm}(\mathbf{r})$ [see Eq. (5)],

$$n(\mathbf{r}) = \sum_i^{\text{occ}} \left(\Phi_i^*(\mathbf{r}) \Phi_i(\mathbf{r}) + \sum_{nm} Q_{nm}(\mathbf{r}) \langle \Phi_i | \beta_m \rangle \langle \beta_n | \Phi_i \rangle \right). \quad (11)$$

Equations (11), (8), and (6) show that the ultrasoft pseudo-wave-functions satisfy a generalized norm-conservation condition

$$\langle \Phi_n | S | \Phi_m \rangle_{R_c} = \langle \Psi_n | \Psi_m \rangle_{R_c}, \quad (12)$$

and this may be used to demonstrate that the logarithmic derivative of the pseudo-wave-functions fits the all-electron value not only at the reference energies, but also around these energies. Finally, the ionic pseudopotential is obtained using an unscreening procedure

$$V_{\text{loc}}^{\text{ion}}(\mathbf{r}) = V_{\text{loc}}(\mathbf{r}) - \int \frac{n(\mathbf{r}')}{|\mathbf{r} - \mathbf{r}'|} d^3r' - V_{\text{xc}}[n(\mathbf{r}) + n_{\text{core}}(\mathbf{r})] \quad (13)$$

and

$$D_{nm}^{\text{ion}} = D_{nm} - \int V_{\text{loc}}(\mathbf{r}) Q_{nm}(\mathbf{r}) d^3r. \quad (14)$$

In actual calculations, it is advantageous to “pseudize” the all-electron wave functions $\Psi_m(\mathbf{r})$ entering the expression for the augmentation functions $Q_{mn}(\mathbf{r})$ [Eq. (5)]. This may be achieved via an expansion in a basis of localized functions⁴⁹ or by replacing the all-electron orbitals $\Psi_m(\mathbf{r})$ by very accurate, “hard-core” norm-conserving pseudo-wave-functions⁵⁴ $\Phi^{\text{NC}}(\mathbf{r})$ with a small augmentation radius R_{aug} .

B. Total energies and Kohn-Sham equations

Variation of the total energy of a solid with respect to the $|\Phi\rangle$ under the constraint

$$N_{\text{el}} = \int n(\mathbf{r}) d^3r = \sum_i^{\text{occ}} \langle \Phi_i | S | \Phi_i \rangle \quad (15)$$

leads to the Kohn-Sham equations

$$\left(T + V_{\text{SC}} + \sum_{nm} \sum_{\alpha} D_{nm}^{\alpha} |\beta_m^{\alpha}\rangle \langle \beta_n^{\alpha}| \right) |\Phi_i\rangle = \epsilon_i S |\Phi_i\rangle, \quad (16)$$

with

$$V_{\text{SC}}(\mathbf{r}) = V_{\text{loc}}^{\text{ion}}(\mathbf{r}) + \int \frac{n(\mathbf{r}')}{|\mathbf{r} - \mathbf{r}'|} d^3r' + \mu_{\text{xc}}[n(\mathbf{r})] \quad (17)$$

[where $V_{\text{loc}}^{\text{ion}}$ and the augmentation part of $n(\mathbf{r})$ are given by the sum over the individual ionic contributions from the sites R_{α}] and

$$D_{nm}^{\alpha} = D_{nm}^{\alpha, \text{ion}} + \int V_{\text{SC}}(\mathbf{r}) Q_{nm}^{\alpha}(\mathbf{r}) d^3r. \quad (18)$$

The solution of the Kohn-Sham equations has been performed using the VASP (Vienna *ab initio* simulation program) which performs a variational solution using a preconditioned conjugate-gradient technique. With the ultrasoft pseudopotential, only a low cutoff energy $E_{\text{cut}} = \frac{\hbar^2}{2m} Q_{\text{cut}}^2$ is necessary. The action of the local potential on the smooth part of the charge density can be calculated using a relatively coarse fast-Fourier-transform (FFT) grid which must contain all the wave vectors up to $Q = 2Q_{\text{cut}}$. Nonlocality is handled in the real-space projection scheme.⁵³ A finer grid is necessary to represent the augmentation charges and the Hartree and exchange-correlation potentials.⁵⁴

One of the consequences of the introduction of ultrasoft pseudopotentials is that the gradients of the energy with respect to the orbitals are now given by

$$|g_n\rangle = (H - \epsilon_n S) |\Phi_n\rangle \quad (19)$$

(for a Hamiltonian that is diagonal in the subspace spanned by the $|\Phi_n\rangle$; for the general case see Ref. 54). The gradient defined this way is no longer orthogonal to the orbitals, i.e., $\langle \Phi_{n'} | S | g_n \rangle \neq 0$. We solve this problem by explicitly orthogonalizing the preconditioned searching vector, using the preconditioning functions K of Ref. 21,

$$|g_n^c\rangle = \left(1 - \sum_{n'} |\Phi_{n'}\rangle \langle \Phi_{n'} | S \right) K |g_n\rangle. \quad (20)$$

The preconditioned gradient is used in conjunction with a sequential band-by-band optimization of the Hamiltonian. After running over all bands, a subspace diagonalization is performed, the Fermi energy is calculated and charge density and potential are updated using a modified Broyden mixing.⁵⁵

Brillouin-zone integrations have been performed on a grid of Monkhorst-Pack special points.⁵⁶ To improve the convergence of the \mathbf{k} -space integrals, we used the finite-temperature version of the LDA,^{51,54,57–59} with the expressions for the electronic free energy, entropy, and fractional occupancy corresponding to a Gaussian broadening of the one-electron levels.^{54,59} The variational quantity is now the free energy; it is minimal with respect

to changes in the orbitals, the chemical potential, and the fractional occupation numbers. The Gaussian broadening greatly improves the convergence of the Brillouin-zone integration and the use of the electronic free energy as the variational quantity, together with fractional occupancies and improved mixing, guarantees the convergence of the iterative eigenvalue determination.

C. Forces on atoms, stresses

For the optimization of the structural parameters, we used a quasi-Newton quench⁶⁰ based on the Hellmann-Feynman forces. It has been shown^{58,59} that even within finite-temperature LDA, the Hellmann-Feynman forces are still given by the derivatives of the energy (not the free energy). This is a consequence of the stationarity properties of the free energy. Due to the dependence of the overlap operator and the augmentation charges on the positions of the ions, additional terms appear in the Hellmann-Feynman forces.⁶¹ For a mixed-basis set, this case was treated by Goedecker and Maschke.⁶² In the same way it is possible to calculate the stresses acting on the unit cell; for details see Ref. 54.

D. Application to the 2p elements C, B, and N

We have performed extensive tests of the accuracy, transferability, and convergence properties of the ultrasoft pseudopotentials for C, B, and N (a small part of the tests for C has been reported in Ref. 47). We used an ultrasoft pseudopotential with two projectors (= two reference energies $\epsilon_{s,p}^{1(2)}$) for the s and p components (cutoff radii $R_{c,s}$ and $R_{c,p}$) and a potential with a single reference energy (radius $R_{c,d}$) for the d component. The augmentation functions for the s and p -wave functions were calculated using a norm-conserving (NC) pseudopotential with small cutoff radii $R_{aug,s}$ and $R_{aug,p}$. Various forms have been tested for the local potential V_{loc} .

For the choice of the local potential, the d pseudopotential or the all-electron potential cut at some small distance gave excellent results. The precise choice of the two reference energies per angular momentum component turned out to be rather uncritical, as long as both energies fall within the energy range of interest. The final choice was for the atomic s and p eigenvalues $\epsilon_{s,p}$ and the second reference energy about halfway between the atomic eigenvalues (equal for the s and p components); the d reference energy has been chosen within the upper region of the valence band, corresponding to an unbound state. With this choice, the logarithmic derivatives of the pseudo-wave-functions at a radius comparable to the interatomic distance in the solid are indistinguishable from the all-electron values over an energy range of ± 15 eV from the atomic eigenvalues.

The augmentation functions are the more accurate the smaller the augmentation radii $R_{aug,i}$ ($i = s, p$). A reduction of $R_{aug,i}$, however, increases the computational effort, since a finer grid for the representation of

the augmentation functions is required. We found that $R_{aug,s} = 1.3$ a.u., $R_{aug,p} = 1.2$ a.u., $R_{aug,d} = 1.3$ a.u. leads to very accurate results. A reduction of all augmentation radii to 1.0 a.u. changes the equilibrium atomic radius of diamond by less than 0.003 a.u., the cohesive energy by less than 0.01 eV/atom, and the bulk modulus by less than 0.005 Mbar.

The most important parameters influencing the transferability and convergence of the pseudopotential are the cutoff radii of the ultrasoft (US) pseudopotentials. The most direct way to test the convergence properties is to perform supercell calculations for a single atom with a plane-wave basis—this allows us to separate neatly convergence and transferability. Figure 1 shows the absolute convergence of the total energy of a C atom (relative to an all-electron calculation) for a norm-conserving PP (with the cutoff radii equal to the augmentation radii) and a series of ultrasoft PP's with varying cutoffs. Each potential is characterized by the value for $R_{c,p}$, and $R_{c,s} = R_{c,p} - 0.2$ a.u. (for $R_{c,p} > 1.6$ a.u.), $R_{c,s} = R_{c,p}$ otherwise, and $R_{c,d} = R_{c,p}$. Convergence within 0.001 eV requires a cutoff energy of $E_{cut} = 1200$ eV for the best ultrasoft potential ($R_{c,p} = 1.4$ a.u.). However, these are unrealistically tight limits. Convergence with 0.01 eV requires a cutoff of ~ 950 eV for the norm-conserving potential, but this is reduced for the ultrasoft potential to 500 eV (for $R_{c,p} = 1.4$ a.u.) and to 230 eV (for $R_{c,p} = 1.8$ a.u.), respectively.

The problematic point with the extremely soft potentials is their transferability. Figure 2 displays the absolute convergence of the cohesive energy of diamond for the same series of pseudopotentials. Convergence within 0.01 eV/atom is achieved at $E_{cut} = 950$ eV for the norm-conserving pseudopotential and $E_{cut} = 600$ eV for the ultrasoft pseudopotential with $R_{c,p} = 1.4$ a.u. In this case the fully converged values agree within 0.005 eV/atom. With a larger cutoff radius, relative convergence may be achieved at even lower energy (e.g., at $E_{cut} = 330$ eV

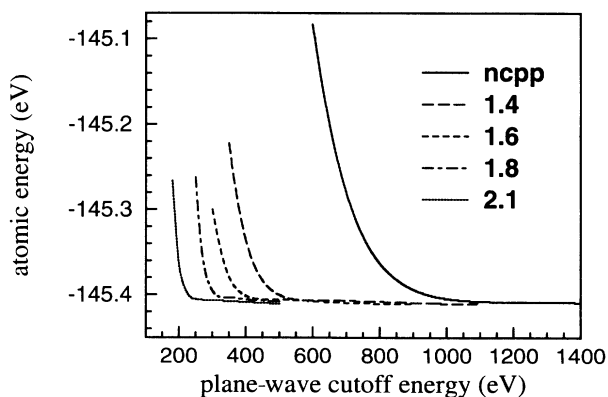


FIG. 1. Convergence of the calculations of the total energy of a free C atom in a basis of plane waves against the cutoff energy E_{cut} , using a norm-conserving (NC) and different ultrasoft (US) pseudopotentials. The US pseudopotentials are characterized by the value of the p cutoff radius (in a.u.); cf. text.

TABLE I. Equilibrium values of the lattice constant a , cohesive energy E_0 , bulk modulus B , and its pressure derivative B' for cubic diamond, calculated using different ultrasoft pseudopotentials and the minimum recommended cutoff energy E_{cut} .

PP	E_{cut} (eV)	a (Å)	E_0 (eV)	B (Mbar)	B'
NC ^a	1100	3.527	9.032	4.61	3.67
US ^b (1.4)	600	3.528	9.026	4.59	3.67
US- d ^c (1.4)	600	3.528	9.026	4.60	3.67
US (1.8)	300	3.532	8.994	4.61	3.65
US- d (1.8)	300	3.530	9.004	4.60	3.64
US (2.0)	240	3.536	8.993	4.67	3.47
US (2.1)	200	3.544	8.899	4.39	3.57
US (2.2)	170	3.544	8.789	4.38	3.67

^aNorm-conserving pseudopotential.

^bUltrasoft pseudopotential with the all-electron potential, cut at a distance of $r = 0.8$ a.u. as the local potential; cutoff radius given in parentheses.

^cUltrasoft pseudopotential with the d -electron pseudopotential as the local potential; cutoff radius given in parentheses.

for $R_{c,p} = 1.8$ a.u. to within 0.02 eV/atom), but the difference in the converged values relative to the norm-conserving potential is now 0.013 eV/atom, indicating a loss in transferability. For extremely large cutoff radii ($R_{c,p} \geq 2.1$ a.u.), transferability is evidently limited. However, other structural and cohesive properties are much less affected than the cohesive energy. Table I summarizes the cohesive properties for diamond, calculated using ultrasoft pseudopotentials with increasing cutoff

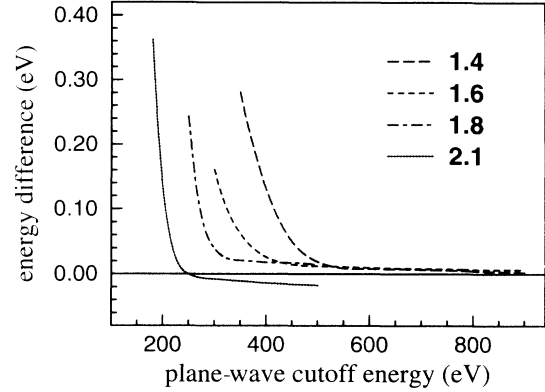


FIG. 2. Convergence of the total energy of diamond (relative to the result obtained using the norm-conserving pseudopotential) for different ultrasoft pseudopotentials. Same notation as in Fig. 1.

radii, different choices for the local part of the potential, and the minimum recommended cutoff energy for each potential. We find that increasing the cutoff radius to a value as large as $R_{c,p} = 2.0$ a.u. (bringing the necessary cutoff energy down to $E_{\text{cut}} = 240$ eV) affects the equilibrium lattice constant by at most 0.2%, the cohesive energy by 0.4%, and the bulk modulus by 1%, i.e., hardly beyond numerical uncertainty (which arises mainly from the interpolation of the energy vs volume data using a Murnaghan equation of state⁶³). Even these small changes in the cohesive energies reflect mostly a constant, structure-independent shift rather than a limitation in the predic-

TABLE II. Structural energy differences ΔE for carbon (in eV/atom), calculated using different pseudopotentials (for nomenclature see Table I).

(a) Energy differences relative to the diamond structure							
Structure	NC	Pseudopotential					
		US (1.4)	US- d (1.4)	US (1.8)	US- d (1.8)	US (2.0)	US (2.1)
fcc	4.6524	4.6485	4.6482	4.6337	4.6401	4.6427	4.5722
bcc	4.3544	4.3510	4.3505	4.3375	4.3433	4.3450	4.2683
sc	2.6354	2.6336	2.6328	2.6284	2.6282	2.6260	2.5873
β -tin	2.7326	2.7307	2.7299	2.7287	2.7268	2.7227	2.6787
bc-8		0.6894	0.6896	0.6889	0.6905	0.6864	0.6768
hexagonal diamond			0.0287		0.0281	0.0293	0.0273
hexagonal graphite		0.0002	-0.0004		0.0028	0.0251	0.0281
(b) Energy difference between hexagonal and rhombohedral graphite (AB vs ABC stacking sequence)							
	NC	US (1.4)	US- d (1.4)	US (1.8)	US- d (1.8)	US (2.0)	US (2.1)
		0.0009	0.0009	0.0008	0.0009	0.0001	0.0022
(c) Energy differences between rhombohedral graphite and cubic diamond (1), and hexagonal graphite and hexagonal diamond (2)							
	NC	US (1.4)	US- d (1.4)	US (1.8)	US- d (1.8)	US (2.0)	US (2.1)
(1)		0.0011	0.0005		0.0037	0.0252	0.0303
(2)			-0.0291		-0.0253	-0.0042	0.0008

TABLE III. Parameters specifying the optimal ultrasoft pseudopotentials for C, B, and N.

Atom (reference configuration)	i (eV)	ϵ_i (a.u.)	$R_{\text{aug},i}$ (a.u.)	$R_{c,i}$
C ($2s^2 2p^2$)	0	-13.84	1.3	1.6
	0	-9.52	1.3	1.6
	1	-9.52	1.2	1.8
	1	-5.31	1.2	1.8
	2	-4.08	1.8	1.8
B ($2s^2 2p^1$)	0	-9.38	1.5	1.8
	0	-6.53	1.5	1.8
	1	-6.53	1.5	1.8
	1	-3.72	1.5	1.8
	2	-2.72	1.8	1.8
N ($2s^2 2p^3$)	0	-18.40	1.2	1.8
	0	-10.88	1.2	1.8
	1	-10.88	1.2	1.8
	1	-7.24	1.2	1.8
	2	-5.44	1.8	1.8

tion of structural phase stability. This is demonstrated in a striking way by the small variations in the structural energy differences compiled in Table II (details of the calculations will be given in the following section). We find that even with cutoff radii as large as $R_{c,p} = 1.8$ a.u., the predicted structural energy differences remain accurate to within 0.01 eV/atom for the large differences between the stable forms of C and the common metallic structures (fcc, bcc, etc.), and 0.003 eV/atom between the actually existing allotropic forms of C (diamond, graphite, bc8). Note that this maximum uncertainty corresponds to a temperature difference of only 35 K. Predictions of this accuracy are possible with ultrasoft pseudopotentials with cutoffs as large as 1.8 a.u. and cutoff energies of only 300 eV. This result is important because it helps to reduce the computational effort involved in *ab initio* calculations of the disordered (liquid, amorphous) phases, of surfaces and interfaces.⁶⁴ For this purpose we have also carried out extensive tests of the convergence of the Hellmann-Feynman forces acting on the atoms in distorted crystalline configurations. For a randomly distorted bc8 structure, for example, we find that the forces calculated using the US(1.8) pseudopotential (and a cutoff of only 300 eV) differ from those calculated using a norm-conserving pseudopotential (and a cutoff of 1100 eV) by at most 0.8% and by 0.4% on average.

Similar, though less extensive tests have been carried out for the pseudopotentials of B and N. Table III compiles the parameters specifying the optimal ultrasoft pseudopotentials for C, B, and N.

III. STRUCTURAL AND ELECTRONIC PROPERTIES OF CARBON

A. Structures

In this section we describe very briefly the crystal structures considered in this work and the relationship between some of them. First, there is the group of tetrahedrally coordinated structures: cubic and hexagonal

diamond and the bc8 structure. Cubic diamond⁵ has a face-centered-cubic Bravais lattice (space group O_h^7) with two atoms in the unit cell at $\pm \frac{a}{8}(1,1,1)$. Each atom has four nearest neighbors forming bond angles of $\cos^{-1}(-\frac{1}{3}) = 109.47^\circ$. The structure may also be viewed as a sequence of layers of buckled hexagonal rings, stacked in an (ABC) sequence in the $[111]$ direction. Changing the stacking sequence to (AB) defines the structure of hexagonal diamond;⁶ it is related to the hexagonal-close-packed structure in the same way as cubic diamond to the fcc structure. The unit cell is hexagonal with four atoms in the basis at positions $\pm\{\frac{1}{3}\mathbf{a}_1, \frac{1}{3}\mathbf{a}_2, z\mathbf{c}\}$, $\pm\{\frac{1}{3}\mathbf{a}_1, \frac{1}{3}\mathbf{a}_2, (\frac{1}{2}-z)\mathbf{c}\}$ where the angle between \mathbf{a}_1 and \mathbf{a}_2 is $\pi/3$. Ideal tetrahedral coordination is achieved for $c/a = \sqrt{8/3}$ and $z = 1/16$. The Bravais lattice of the bc8 structure^{23,24} is body-centered cubic with eight atoms at positions $\pm a(x, -x, x)$, $\pm a(-x, -\frac{1}{2} + x, x)$, $\pm a(\frac{1}{2} - x, -x, -x)$, $\pm a(x, x, \frac{1}{2} - x)$, space group T_7^h . x is a free parameter; for $x = 0.1036$ coordination is almost tetrahedral, and for all other values of x one has to differentiate between one A -type and three B -type bonds (with $d_A < d_B$ for $x < 0.1036$, and $d_A > d_B$ for $x > 0.1036$).

The second group consists of the hexagonal and rhombohedral graphite structures.^{3,4} Both forms of graphite consist of honeycomb nets, with an AB stacking sequence (the atoms of the B layer centering half of the hexagons of the A layer) for the hexagonal form, and an ABC sequence for the trigonal form. Simple geometrical relationships exist between rhombohedral graphite and cubic diamond, and the hexagonal polymorphs of both graphite and diamond. It is possible to deform rhombohedral graphite continuously into cubic diamond²⁷ by decreasing the interlayer bond length ($D = 3.35$ Å in the graphitic phase) while increasing the intralayer bond length (initially $d = 1.54$ Å) and the angle between the interlayer and intralayer bonds (from $\theta = 90^\circ$ toward $\theta = 109.47^\circ$). All the intermediate structures have rhombohedral (D_{3d}^5) symmetry. A similar transformation path links hexagonal graphite and hexagonal diamond. The actual transformation will occur along the path minimizing the energy barrier as a function of D , d , and θ .

The third group of structures are the sixfold-coordinated simple cubic and β -tin structures (derived from the cubic diamond lattice by a tetragonal distortion), and as the fourth group we consider the common cubic metallic structures: cubic face and body centered.

For the Brillouin-zone integrations we used the Monkhorst-Pack special-point technique⁵⁶ and a Gaussian broadening of the one-electron levels with $\sigma = 0.1$ eV (cf. Sec. IIB) with all energies extrapolated to $\sigma = 0$. For the cubic and hexagonal diamond structures, the bc8 structure, the hexagonal and trigonal graphite lattices, the sc and β -tin structures, and the fcc and bcc structures we used 10, 14, 7, 28, 15, 56, 56, 66, and 44 \mathbf{k} points in the irreducible part of the Brillouin zone, respectively.

B. Calculated structural and cohesive properties

Table IV summarizes the calculated structural and cohesive properties [we show only the results for the

TABLE IV. Structural and cohesive properties of C in various phases: atomic volume V , lattice constants a, c [to facilitate comparison (c/a) is given as the ratio of the interlayer distance to the lattice constant a], structural parameters (x, z), cohesive energy E_0 , bulk modulus B , pressure derivative B' , and energy difference ΔE relative to the cubic diamond structure.

Cubic diamond						
	US-1.4	US-1.8	Fahy <i>et al.</i> ^a	Biswas <i>et al.</i> ^b	McMahan ^c	Expt. ^d
V [\AA^3]	5.488	5.498	5.583	5.571	5.59	5.673
a [\AA]	3.528	3.530	3.548	3.545	3.55	3.567
E_0 [eV/atom]	-9.026	-9.004	-8.17	-8.43	-7.35	
B [Mbar]	4.60	4.60	4.44	4.94	4.64	4.43
B'	3.67	3.64	3.24	2.60		~ 4
ΔE [eV/atom]	0	0	0	0	0	
Hexagonal diamond						
	US-1.4	US-1.8	Fahy <i>et al.</i> ^a			Expt. ^d
V [\AA^3]	5.504	5.513	5.602			5.61-5.67
a [\AA]	2.480	2.483	2.50			2.51-2.52
c/a	0.833	0.832	0.828			0.819
z	0.0625	0.0625	0.0625			0.0625
E_0 [eV/atom]	-8.998	-8.976	-8.140			
B [Mbar]	4.62	4.66	4.40			
B'	3.66	3.64	3.5			
ΔE [eV/atom]	0.028	0.028	0.030			
Hexagonal graphite						
	US-1.4	US-1.8	Yin and Cohen ^f	Jansen and Freeman ^e		Expt. ^d
V [\AA^3]	8.609	8.627	9.312	8.939		8.734-8.797
a [\AA]	2.440	2.443	2.47	2.459		2.46
c/a	1.369	1.367	1.362	1.388		1.35-1.365
E_0 [eV/atom]	-9.027	-9.001				-7.374
B [Mbar]	2.86	2.88	2.361	3.19		2.86-3.19
B'	3.57	3.58				
ΔE [eV/atom]	-0.0004	0.0028	0.0001			
Rhombohedral graphite						
	US-1.4	US-1.8	Fahy <i>et al.</i> ^a			
V [\AA^3]	8.531	8.550	8.50			
a [\AA]	2.440	2.443				
c/a	1.356	1.354				
E_0 [eV/atom]	-9.026	-9.000				
B [Mbar]	2.89	2.93				
B'	3.51	3.52				
ΔE [eV/atom]	0.0005	0.0037	0.009			
bc-8 structure						
	US-1.4	US-1.8	Yin and Cohen ^f	Fahy <i>et al.</i> ^a	Biswas <i>et al.</i> ^b	
V [\AA^3]	5.392	5.397	5.733	5.456	~ 4.65	
a [\AA]	4.419	4.420	4.51	4.436		
x	0.09425	0.09434	~ 0.1003			
E_0 [eV/atom]	-8.336	-8.313		-7.48		
B [Mbar]	4.18	4.20	4.00	4.11		
B'	3.88	4.11		3.7		
ΔE [eV/atom]	0.689	0.691		0.690	~ 0.7	
β -tin structure						
	US-1.4	US-1.8	Yin and Cohen ^g			
V [\AA^3]	5.234	5.234	5.553			
a [\AA]	3.310	3.310				
c/a	0.390	0.390				
E_0 [eV/atom]	-7.425	-7.406				
B [Mbar]	3.99	3.98				
B'	3.83	3.76				
ΔE [eV/atom]	2.730	2.727	2.82			

TABLE IV. (Continued).

Simple cubic				
	US-1.4	US-1.8	Yin and Cohen ^g	McMahan ^c
V [\AA^3]	5.304	5.305	5.543	5.423
a [\AA]	1.744	1.744	1.770	1.757
E_0 [eV/atom]	-7.522	-7.505		
B [Mbar]	3.99	3.98		
B'	3.83	3.76		
ΔE [eV/atom]	2.633	2.628	2.66	2.60
Body-centered cubic				
	US-1.4	US-1.8	Yin and Cohen ^g	McMahan ^c
V [\AA^3]	6.290	6.315	6.700	6.479
a [\AA]	2.326	2.329	2.375	2.349
E_0 [eV/atom]	-4.676	-4.661		
B [Mbar]	2.18	2.18		
B'	3.96	3.96		
ΔE [eV/atom]	4.351	4.343	4.28	4.24
Face-centered cubic				
	US-1.4	US-1.8	Yin and Cohen ^g	McMahan ^c
V [\AA^3]	6.890	6.927	7.290	7.256
a [\AA]	3.021	3.026	3.078	3.073
E_0 [eV/atom]	-4.378	-4.364		
B [Mbar]	1.70	1.683		
B'	2.80	2.51		
ΔE [eV/atom]	4.648	4.640	4.59	4.50

^aReferences 27, 28, PP.

^bReferences 8, 25, PP.

^cReference 29, LMTO.

^dExperimental data as given in Refs. 5, 65–69.

^eReference 30, FLAPW.

^fReferences 23, 24, PP.

^gReference 7, PP.

US- $d(1.4)$ and US- $d(1.8)$ pseudopotentials] and compares them with previous calculations and experimental data compiled from Refs. 65–69. For the diamond and graphite structures, our calculations underestimate the lattice constant by about 1%, they overestimate the cohesive energy by about 20%, the bulk modulus of diamond is overestimated by about 4%, and that of graphite is correct to within the experimental uncertainty. The slight overbinding present in our calculations is characteristic for the LDA. It is somewhat smaller in the calculations of Fahy *et al.*,^{27,28} Yin *et al.*,^{7,23,24} and Biswas *et al.*,^{8,25} due to the use of a different exchange-correlation functional. The Wigner-interpolation formula⁷⁰ generally predicts weaker overbinding effects, but is certainly less accurate than the Ceperley-Alder functional⁷¹ used in our calculations. In the hexagonal structures we have varied the axial ratio, and for the hexagonal diamond structure also with respect to z , for the bc-8 structure we have minimized the energy with respect to the parameter x .

C. Structural phase stability

The most important result is certainly the prediction of the relative phase stability, as expressed by the struc-

tural energy differences given in Tables II and IV and as expressed by the energy vs volume curves shown in Fig. 3. Our calculations with the most accurate pseudopotential predict that at zero pressure the energy difference between cubic diamond, and hexagonal and trigonal graphite is zero within the high accuracy of the calculations ($|\Delta E| \leq 0.001$ eV/atom ~ 10 K). This agrees with the pseudopotential calculations of Yin and Cohen²⁴ [ΔE (hexagonal graphite-diamond) $\simeq 0.0014$ eV/atom], whereas according to Fahy *et al.*²⁷ the binding energy of diamond with respect to graphite is overestimated by 0.009 eV/atom. One has to emphasize that the difference in the cohesive energies is smaller than the difference in the zero-point vibrational energies calculated from the theoretical phonon densities of state of graphite⁷² and diamond⁷³ [$E_{\text{vib}}(\text{graphite}) = 0.1659$ eV/atom, $E_{\text{vib}}(\text{diamond}) = 0.1809$ eV/atom; $\Delta E_{\text{vib}} = 0.0150$ eV/atom]. There is also only an extremely small energy difference between the hexagonal and trigonal stacking variants of graphite (under pressure the trigonal phase becomes even lower in energy; see Fig. 3), whereas the hexagonal form of diamond is higher in energy by 0.028 eV/atom, again in very good agreement with the result of Fahy *et al.*^{27,28} Of the other structures covered in our study, bc-8 is about 0.69 eV/atom higher in en-

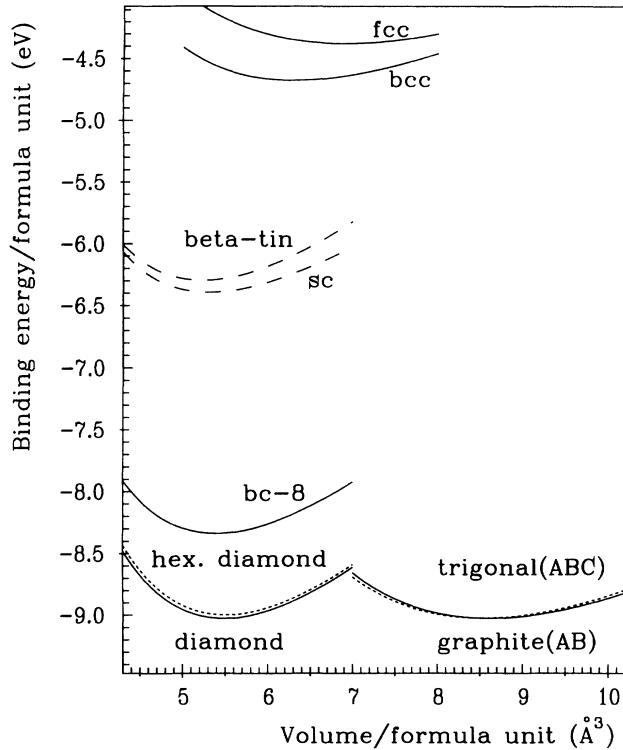


FIG. 3. Energy vs volume for C in the cubic and hexagonal diamond structures, in the hexagonal and trigonal graphite structures, in the β -tin, the bc-8, and the simple, body-centered-, and face-centered-cubic structures.

ergy (again in excellent agreement with the work of Fahy *et al.*^{27,28} and Biswas *et al.*²⁵); for the sc and β -tin structures ΔE is of the order 2.6–2.7 eV/atom, and for the fcc and bcc structures we find $\Delta E \sim 4.3$ –4.65 eV/atom. We think that it is quite remarkable that the present set of structural energies agrees so well with the data obtained with very different approaches. The very large differences in the structural energies reflect the strong preference for sp^3 - and sp^2 -type bonds, but the difference between the sp^3 and sp^2 bond energies is compensated almost entirely by the difference in the promotion energies.

D. Graphite-diamond transition

A central question is the energy barrier for the transformation between the energetically almost degenerate tetrahedral and layered phases. The transitions between the hexagonal phases of graphite and diamond, and between rhombohedral graphite and cubic diamond may be described by calculating the total energy of a general hexagonal structure with four atoms per cell, respectively a rhombohedral structure with two atoms per cell (equivalent to a hexagonal cell with six atoms) as a function of the volume and the axial ratio c/a of the cell and the parameter z specifying the buckling of the hexagonal layers. In the rhombohedral cell the six atomic positions are (in units of the hexagonal

basis vectors) $(0,0,0)$, $(1/3,1/3,1/3)$, $(-1/3,-1/3,2/3)$, $(0,0,1/3-\eta z)$, $(1/3,1/3,2/3-\eta z)$, and $(-1/3,-1/3,-\eta z)$ with $z = 1/12$. $\eta = 0$ corresponds to the rhombohedral graphite structure and no buckling of the honeycomb layers; $\eta = 1$ corresponds to the cubic diamond lattice. Varying η between $\eta = 0$ and $\eta = 1$ and minimizing for each given value of η the total energy with respect to the axial ratio c/a (and hence with respect to the inter-layer distance) and to the volume of the cell defines a path describing a continuous transformation from rhombohedral graphite to cubic diamond. Similar calculations have been performed by Fahy *et al.*²⁷ and Kertesz and Hoffmann⁷⁴ who treated the bond length between the layers as the independent variable. Figure 4 describes the variation of the total energy, volume, and axial ratio as a function of the degree of buckling of the graphitic layers. The calculations have been performed using the US-1.4 and US-1.8 pseudopotentials. The calculations predict an energy barrier of $\Delta E = 0.324$ eV/atom and $\Delta E = 0.325$ eV/atom, respectively (relative to cubic diamond); the saddle point is situated roughly at $\eta = 0.5$ and an axial ratio of $c/a \simeq 2.79$ [to be compared with $(c/a) = 2.45 = \frac{3}{2}\sqrt{8/3}$ for diamond and $(c/a) = 4.07$ for trigonal graphite]. This value represents an upper bound for the actual energy barrier: On a transformation-path-violating rhombohedral symmetry, the barrier might ac-

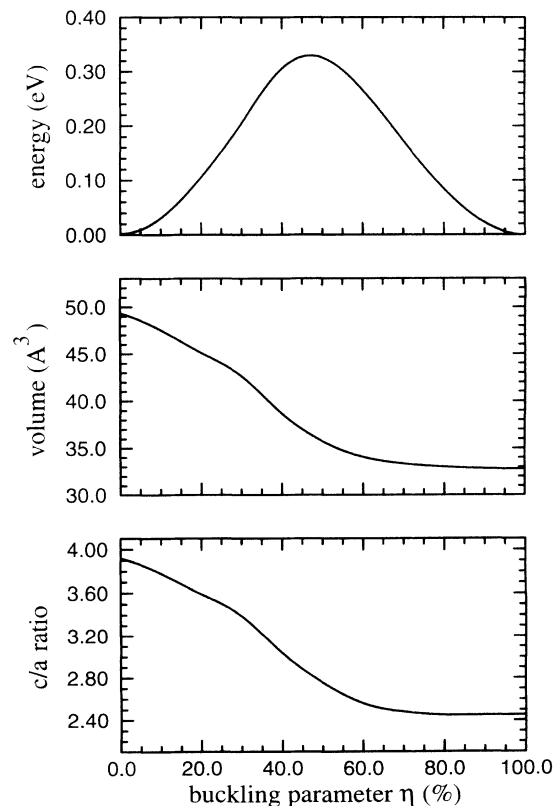


FIG. 4. Variation of the total energy, volume, and axial ratio of the hexagonal cell as a function of the degree of buckling of the graphitic layers, describing a continuous deformation from trigonal graphite to cubic diamond (cf. text).

tually be lower. Both the energy barrier and the calculated structure at the saddle point are in excellent agreement with the results of Fahy *et al.*²⁷ The essential result of both studies is that, starting from the layered phase, buckling and interlayer distance are strongly correlated: Any deformation of the layers induces a rapid decrease of the interlayer distance and vice versa, until the saddle point has been reached. After the saddle point, the deformation consists mainly in a change of the bond length within the layers.

E. High-pressure phase transitions

Unlike Si and Ge, which transform to the sixfold-coordinated β -tin structure under moderate compression, C does not show a transition to sixfold coordination. On the other hand, it has been claimed that the bc8 structure (which is formed in Si as a metastable phase on unloading the high-pressure β -tin phase to ambient pressure) exists as a high-pressure phase of C.^{23–25,28} In our calculations we have also considered the possibility of a high-pressure phase transition and confirmed the existence of a diamond-bc8 transition (Fig. 5). The transition pressure determined by the common-tangent construction is $p_t \simeq 10$ –11 Mbar; the volume change at the transition is $\Delta\Omega = -0.08 \text{ \AA}^3/\text{atom}$ (Table V), again in very good agreement with previous calculations.^{23,28,25}

F. Electronic properties

The electronic band structures of the tetragonal and layered phases of C (and for comparison that of the corresponding phases of BN; cf. Sec. IV) are shown in Figs. 6–9. It is not necessary to comment on the band structure of cubic diamond in much detail. The fundamental gap is $E_g = 4.25 \text{ eV}$ from Γ to $\sim 0.8X$, in good agreement with the calculation of Fahy and Louie²⁸ ($E_g = 4.3 \text{ eV}$). The calculation of Fahy and Louie is based on PP's and a localized s, p basis and the authors note a reduction of the gap to $E_g = 3.9 \text{ eV}$ if d states are included in the basis.^{28,75} The present calculations use a well-converged PW basis. Compared to experiment⁷⁶ ($E_g = 5.47 \text{ eV}$), the calculation shows the underestimate of the gap characteristic for the LDA. We believe that the differences between the two sets of calculations are to be attributed

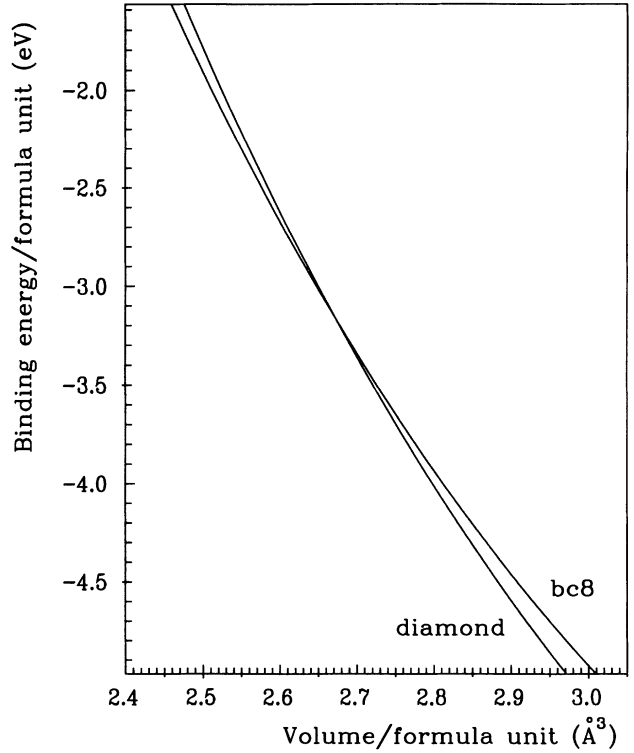


FIG. 5. Total energy vs volume of the diamond and bc8 structures at very large compression.

to our use of a more accurate exchange-correlation functional. In the hexagonal diamond structure, the width of the valence band is essentially unchanged but the fundamental gap (indirect, $\Gamma \rightarrow K$) is reduced to $E_g = 3.05 \text{ eV}$ (to be compared with the value $E_g = 3.3 \text{ eV}$ quoted by Fahy and Louie²⁸). On the other hand, even quite recently there has been an intense interest in the band structure of graphite.^{26,30,77} The recent interest arose from the fact that FLAPW (Ref. 30) and pseudopotential calculations^{26,75,77,78} differ in the position of the top of the σ band, with the FLAPW calculations being in better agreement with experiment.^{79,80} Table VI summarizes the results for characteristic one-electron energies (bottom and top of σ, σ^*, π bands, etc.). The results are relevant in several respects: (a) The comparison of the

TABLE V. High-pressure phase transition diamond \rightarrow bc8. Transition pressure p_t , initial and final atomic volumes and volume change at the transition ($V_i, V_f, \Delta V$).

	Present work			Previous work	
	US-1.4	US-1.8	Yin ^a	Fahy and Louie ^b	Biswas <i>et al.</i> ^c
p_t (Mbar)	10.95	10.20	12.00	11.10	12.00
V_i (\AA^3)	2.71	2.80	2.62	2.75	
V_f (\AA^3)	2.63	2.71	2.55	2.63	
ΔV (\AA^3)	-0.08	-0.09	-0.12	-0.06	

^aReference 23.

^bReference 28.

^cReference 25.

TABLE VI. Characteristic electron energy eigenvalues (in eV) of graphite, evaluated relative to the Fermi level. Comparison of present results with previous calculations and experiment.

	Present work		Previous calc.			Expt.
	US-1.4	US-2.0	Ref. 30	Ref. 26	Ref. 77	
	US-1.8		FLAPW	PP	PP	
Bottom σ	-19.7	-19.7	-19.6	-20.1	-19.5	-20.6 ^a
	-19.35	-19.35	-19.3	-19.8	-19.0	
Bottom π	-8.8	-8.8	-8.7	-8.9	-8.6	-8.1, ^a -8.5 ^b
	-6.7	-6.7	-6.7	-6.8	-6.7	-5.7, ^a -7.2 ^b
Top σ	-3.05	-3.0	-4.6	-3.5	-3.0	-4.6, ^a -5.5 ^b
	-3.0	-3.0	-4.6	-3.5	-3.0	
Empty σ^*	3.8	3.8	3.8	3.7	4.0	
	8.5	8.6	8.3	7.9	8.5	6.9 ^a

^aReference 79.

^bReference 80.

calculations based on different ultrasoft pseudopotentials show that even with very soft pseudopotentials ($R_c = 2.0$ a.u.) and very low cutoff energies, complete convergence of the one-electron energies may be achieved. (b) Except for the critical eigenvalue describing the top of the σ band, the present results agree even better with the FLAPW result of Jansen and Freeman³⁰ than other pseudopotential calculations. The exception is the position of the top of the σ band. Jansen and Freeman attributed

the discrepancy with previous PP calculations to an insufficient \mathbf{k} point sampling. Our calculations (28 special \mathbf{k} points) and that of Schable and Martins⁷⁷ (6–40 special \mathbf{k} points) are undoubtedly based on a fully converged \mathbf{k} -point mesh so that the reason for the discrepancy remains unclear.

The band structure of rhombohedral graphite differs from that of the hexagonal stacking variant by (a) the presence of a small direct gap (along K - H) of $E_g \sim 0.8$

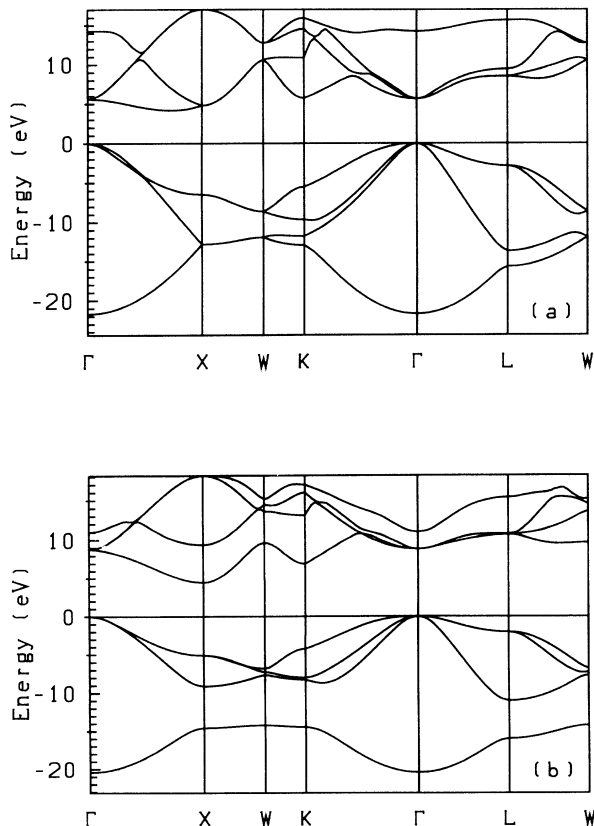


FIG. 6. The electronic band structure of C in the diamond (a) and of BN in the zinc-blende (b) structure.

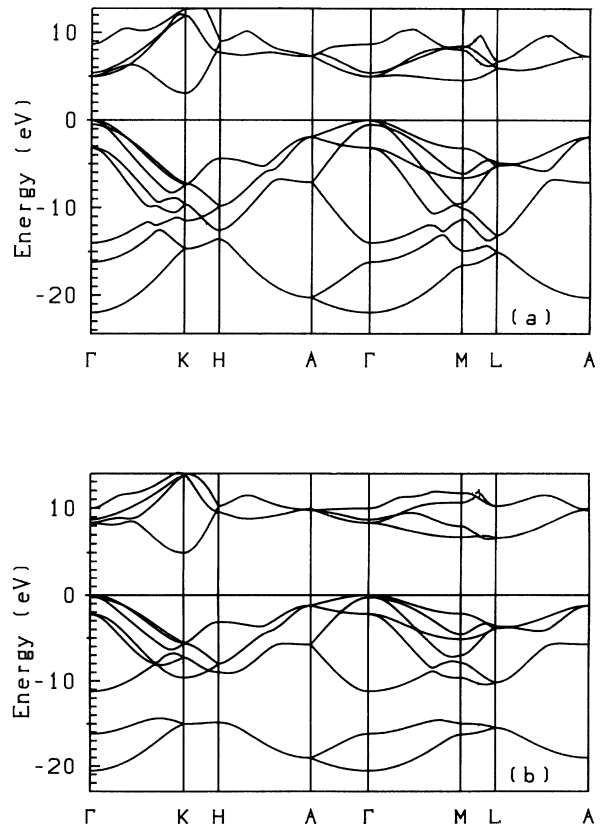


FIG. 7. The electronic band structure of C in the hexagonal diamond (a) and of BN in the wurtzite (b) structure.

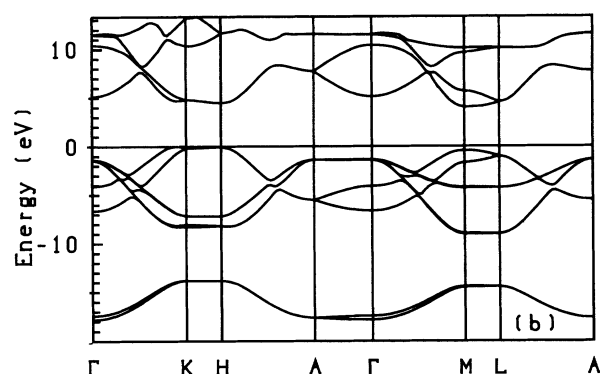
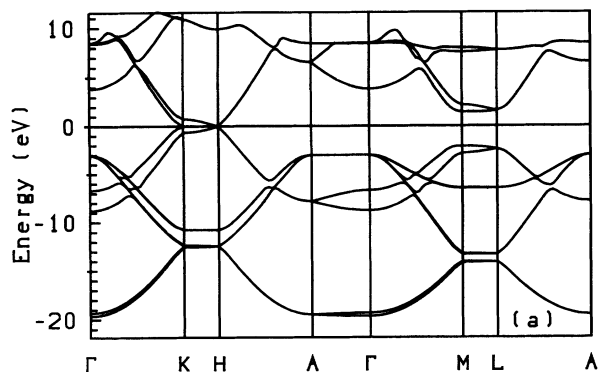


FIG. 8. The electronic band structures of hexagonal graphite (a) and BN (b).

eV, whereas hexagonal graphite is a semimetal. (b) The top of the σ band (at the L point) is raised to ~ -1.7 eV. The existence of a narrow gap agrees with the results of Fahy *et al.*²⁷ It is important for understanding the semiconductorlike transport properties of pyrolytic graphite (which contains a certain fraction of rhombohedral graphite) compared to the semimetallic properties of hexagonal graphite.

IV. STRUCTURAL AND ELECTRONIC PROPERTIES OF BORON NITRIDE

A. Structures

Assuming the electronic configuration $B^{-}N^{+}$, the compound BN is isoelectronic to the element C, and this similarity is reflected in the structures of the known polymorphic forms of BN. Like C, BN exists in layered and fourfold-coordinated phases. The common form of layered BN has a hexagonal structure (space group D_{6h}) with four atoms in the unit cell.⁹ It exhibits an $AA'AA'$... stacking sequence such that the boron atoms in layer A are placed directly below the nitrogen atoms in layer A' . This is different from the hexagonal form of graphite with $ABAB$... stacking, where only half of the carbon atoms are directly above

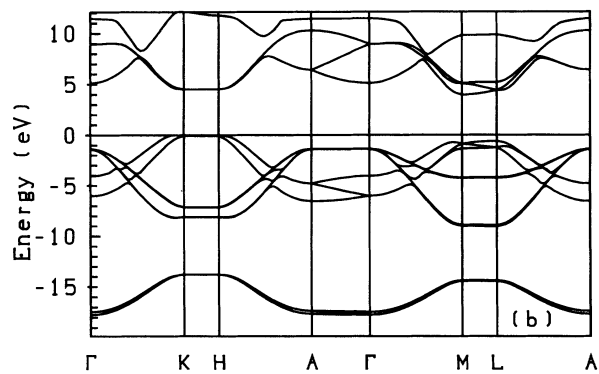
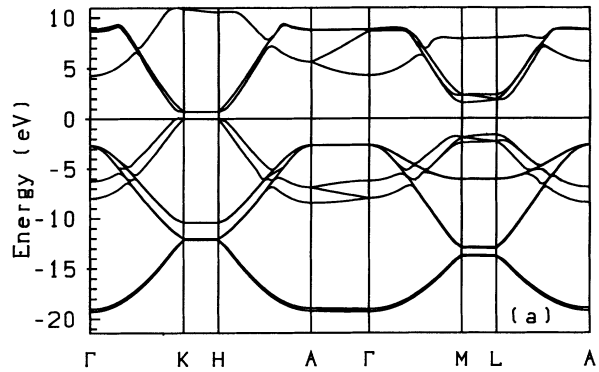


FIG. 9. The electronic band structures of rhombohedral graphite (a) and BN (b).

or below the carbon atoms in the adjacent layers. The rhombohedral form of layered BN (space group C_{3v}) has a three-layer $ABCABC$ stacking sequence similar to hexagonal graphite. The denser forms of BN crystallize in the zinc-blende and wurtzite structures of which cubic and hexagonal diamond are just the homopolar analogs. Zinc-blende BN (z -BN) may be synthesized under pressure and elevated temperature from rhombohedral BN (r -BN), and wurtzite-BN (w -BN) from hexagonal BN (h -BN) (at somewhat lower temperatures).^{10,11} The transformations may be described in the same way as the transformations between the layered and tetrahedral phases of C in terms of a progressive buckling of the honeycomb layers, accompanied by a change of the axial ratio and volume of the hexagonal cell. Finally, we have also calculated the total energy of BN in the rock-salt structure — again there is a simple analogy with the simple cubic phase of C (which may be considered as the homopolar analog of rocksalt-BN).²⁸

B. Cohesion and phase stability

Table VII summarizes the calculated cohesive and structural properties of BN in the hexagonal and rhombohedral layered structures, and in the zinc-blende,

wurtzite, and rocksalt structures. Figure 10 shows the energy of the competing phases as a function of volume. In our calculations we have used the optimized ultrasoft pseudopotentials for B and N described in Table III (cutoff energy $E_{\text{cut}} = 300$ eV). In addition, several calculations with a much harder norm conserving potential with smaller cutoff radii ($R_{c,l} = 1.2$ a.u. for N and $R_{c,l} = 1.5$ a.u. for B, $l = s, p, d$) and a very high cutoff energy of $E_{\text{cut}} = 1600$ eV have been performed to control convergence and transferability of the pseudop-

entials. The calculations use again the Ceperley-Alder exchange-correlation functional and the Monkhorst-Pack special-point method and Gaussian broadening ($\sigma = 0.1$ eV and extrapolation to $\sigma = 0$) for Brillouin-zone integration. For the zinc-blende and rocksalt structures 10 special points have been used, and 5, 15, and 14 points for the hexagonal, rhombohedral, and wurtzite phases, respectively.

Compared to C, the phase stability of BN has been studied much less extensively. Structural energy differ-

TABLE VII. Structural and cohesive properties of BN in various phases: atomic volume V , lattice constants a, c [to facilitate comparison between the different structures (c/a) is given as the ratio of the interlayer distance to the lattice constant a], buck modulus B , pressure derivative B' , cohesive energy E_0 , and structural energy difference ΔE relative to the zinc-blende structure.

	Present work		Wentzovitch <i>et al.</i> ^a	Park <i>et al.</i> ^b	Xu and Ching ^c	Expt. ^d
	NC	US				
Zinc-blende						
V [\AA^3]	5.702	5.718	5.860	5.785	5.905	5.930
a [\AA]	3.573	3.576	3.606	3.59	3.615	3.615
E_0 [eV/atom]	-8.185	-8.152	-7.15		-7.00	-6.6
B [Mbar]	3.95	3.97	3.67	3.54	3.70	3.69–4.65
B'	3.67	3.59			3.80	~ 4
ΔE [eV/atom]	0	0	0	0	0	
Wurtzite						
V [\AA^3]		5.731			5.845	
a [\AA]		2.521		2.56	2.536	2.55
c/a		0.826			0.828	0.824
E_0 [eV/atom]		-8.132			-6.925	
B [Mbar]		4.01		3.49	3.90	
B'		3.59			6.30	
ΔE [eV/atom]		0.020	0.027		0.075	
Hexagonal (AA')						
V [\AA^3]	8.617	8.613			8.970	9.012
a [\AA]	2.481	2.486			2.494	2.50
c/a	1.304	1.295			1.335	1.332
E_0 [eV/atom]	-8.133	-8.097			-7.350	
B [Mbar]	2.52	2.61			3.35	
B'	3.58	3.66			3.76	
ΔE [eV/atom]	0.052	0.055	0.06		-0.35	
Rhombohedral (ABC)						
V [\AA^3]		8.603				
a [\AA]		2.495				
c/a		1.294				
E_0 [eV/atom]		-8.100				
B [Mbar]		2.62				
B'		3.87				
ΔE [eV/atom]		0.052	0.06			
Rocksalt						
V [\AA^3]	5.168	5.168				
a [\AA]	3.458	3.458	3.493			
E_0 [eV/atom]	-6.451	-6.429	-5.45			
B [Mbar]	4.12	4.16	4.25			
B'	3.76	4.00				
ΔE [eV/atom]	1.734	1.723	1.70			

^aReferences 33–35.

^bReference 37.

^cReference 38.

^dAs compiled in Refs. 33–38.

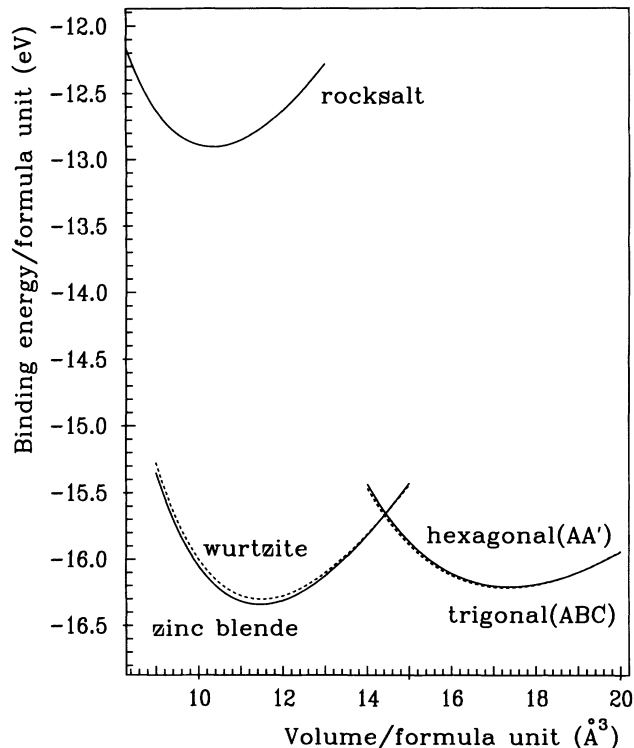


FIG. 10. Energy vs volume for BN in the zinc-blende, wurtzite, hexagonal, trigonal, and rocksalt structures.

ences have been calculated by Wentzcovitch *et al.*^{33–35} and Xu and Ching,³⁸ with very different results: Whereas Wentzcovitch *et al.* predict the close-packed phases to be more stable than the layered phases [$\Delta E(h\text{-BN}-z\text{-BN}) = 0.06$ eV/atom ~ 700 K], Xu and Ching³⁸ predict the hexagonal phase to be *much* more stable [$\Delta E(h\text{-BN}-z\text{-BN}) = -0.35$ eV/atom ~ 4000 K]. Our results for binding energy, lattice constants, and bulk modulus are in good agreement with experiment; they show the overbinding effects ($\Delta a \sim -1\%$, $\Delta E_0 \gtrsim +10\%$) characteristic for the LDA. That the results of Wentzcovitch *et al.* are slightly closer to experiment has to be attributed to the use of the less accurate Wigner-interpolation formula for exchange and correlation (the exchange-correlation potential used in the FLAPW calculations of Park *et al.*³⁷ and the orthogonalized linear combination of atomic orbitals (OLCAO) calculations of Xu and Ching³⁸ has not been specified in their papers). A noticeable point is that our calculation predicts a large difference in the bulk moduli of the dense ($B \sim 4$ Mbar) and the layered phases ($B \sim 2.6$ Mbar) as expected, whereas in Xu and Ching's³⁸ calculation this difference is only about 10%.

The most interesting result is of course the complete set of structural energy differences. The comparison of the results obtained with a relatively hard potential (and a very large cutoff) shows that the results obtained with the optimized ultrasoft potential are well converged. Our structural energy differences are in excellent agreement with those obtained by Wentzcovitch *et al.*^{33–35} using a mixed-basis pseudopotential technique. In particular, both calculations predict the zinc-blende structure to be about 0.05 – 0.06 eV/atom lower in energy than either

of the layered phases. This difference is distinctly larger than the difference between the layered and dense phases of carbon (which is almost zero). This suggests that the partially ionic character of BN affects the bonding of the layered phases more than that of the dense phases. Also, the energy difference between zinc-blende and wurtzite BN is slightly larger than between cubic and hexagonal diamond. The prediction that the electronic ground-state energy of *z*-BN is lower than that of *h*-BN means that the observed stability of the layered phases must be attributed to differences in the phonon energies. However, in contrast to diamond and graphite, the phonon densities of state are unknown for the BN polytypes. Wentzcovitch *et al.*³⁵ have estimated the zero-point vibrational energies from the low-temperature specific heats within a two-dimensional (2D) Debye model for the layered and a 3D Debye model for the tetrahedral phases. With Debye temperatures of $\Theta(h\text{-BN}) \simeq 600$ K and $\Theta(z\text{-BN}) \simeq 1700$ K, the resulting difference in the zero-point vibrational energies is $\Delta E_{\text{vib}} = -0.15$ eV/atom, which would overcompensate the difference in the electronic ground-state energies. However, for carbon, a calculation of ΔE_{vib} from a crude model of the full phonon densities of state yields a difference in the zero-point vibrational energies which is one order of magnitude smaller. Hence, the reason for the observed phase stability of *h*-BN remains to be clarified. A full calculation of the vibrational spectrum would be necessary.

1. Transformation between rhombohedral and zinc-blende BN

We have also calculated the energy along a transformation path taking the rhombohedral into the zinc-blende form (see also Sec. III B 3 for the corresponding transformations in C). The change in energy follows essentially the same characteristics as in carbon (Fig. 11): Even a modest buckling of the layers leads to a large change in volume and interlayer distance until the saddle point is reached. After the saddle point, the volume and shape of the cell change only modestly. The energy barrier for the transformation is only half as large as in carbon, $\Delta E = 0.16$ eV/atom relative to *r*-BN.

2. High-pressure phase transitions

At very high pressure, the rocksalt structure becomes energetically more favorable than the zinc-blende phase. The transition pressure is calculated to be $p_t = 11.7$ Mbar; the atomic volume before and after the transition is 50% and 48%, respectively, of the equilibrium volume of *z*-BN. This is in good agreement with the pressure and volume for the transition calculated by Wentzcovitch *et al.*³⁴ ($p_t = 11.1$ Mbar, $V_i = 0.45V_0$, $V_f = 0.42V_0$).

C. Electronic structure

Figures 6–9 compare the band structures of the corresponding phases of BN and C; Table VIII summarizes the

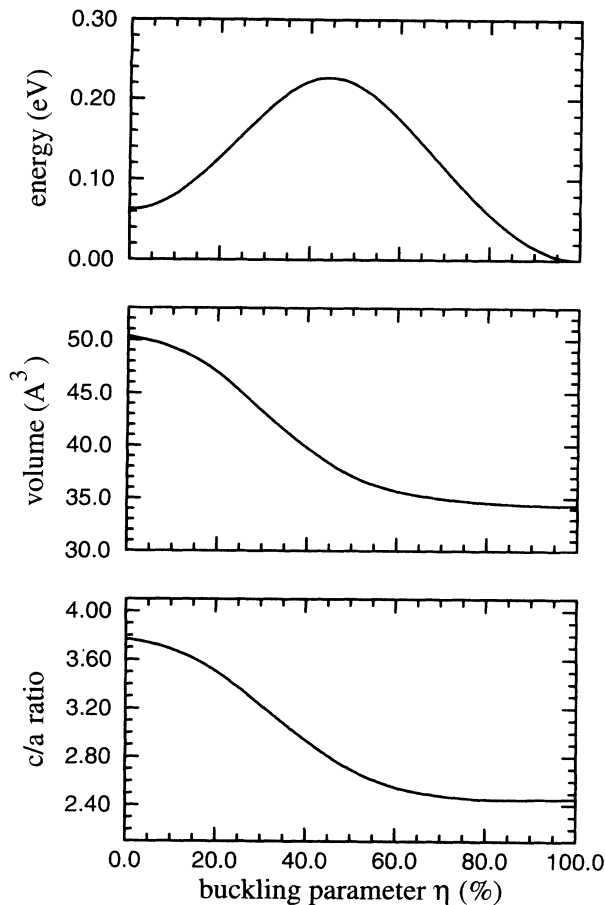


FIG. 11. Variation of the total energy, volume, and axial ratio of the hexagonal cell as a function of the degree of buckling of the hexagonal layers, describing the transformation from rhombohedral (trigonal) to zinc-blende BN.

important features of the band structure (bandwidths, gaps), comparing theory and experiment (compiled from Refs. 81–87). In the older literature, widely conflicting results may be found (cf. the summary given in Ref. 33 for z -BN, and in Ref. 36 for h -BN). For z -BN, the present results using ultrasoft pseudopotentials and a plane-wave basis are in very good agreement with pseudopotential mixed-basis³³ and FLAPW (Ref. 37) results; small differences exist with the OLCAO calculations.³⁸ All calculations agree in characterizing z -BN as a semiconductor with an indirect gap (Γ - X) of 4.2–4.4 eV and a width of the valence band of 20.1–20.4 eV. Compared to experiment, the width of the gap is underestimated by about 2 eV—this discrepancy is characteristic for the limitations of the LDA. Compared to cubic diamond, there is almost no change in the width of the gap and in total width of the valence band. The partially ionic character of BN leads to the opening of a gap in the valence band of 3.2 eV ($W \rightarrow L$) separating the σ and π valence bands. The lower part of the valence band is dominated by N $2s$ states and the upper part by B and N p states, the B s states contributing to both parts of the valence band. The weaker hybridization is responsible for the lower cohesive energy and bulk modulus of w -BN compared to

diamond. The wurtzite phase is also predicted to be an indirect-gap semiconductor, with a slightly larger gap of 4.9 eV—again we note a good agreement with the FLAPW results of Park *et al.*³⁷

The difference in the electronic properties of C and BN is greater in the layered phases: h -BN is a good insulator, whereas graphite is a semimetal. There is considerable disagreement, however, on the width and character of the fundamental gap. Optical absorption studies^{84,85} describe h -BN as a direct-gap semiconductor with a gap ranging between 3.8 and 5.8 eV, the large discrepancy being attributed to the different quality of the samples. From reflectivity measurements,^{86–87} a width of the gap of 5.0–5.7 eV has been deduced. Our calculations predict a direct gap at the M point of 4.5 eV, which is 0.4 eV larger than the indirect gap between the M and H points (Table VIII). Figure 9(b) shows the band structure of h -BN. Compared to graphite, the individual widths of the bonding σ and π bands are strongly reduced due to the presence of the internal gap in the heteropolar material (note that the internal σ - π gap in the valence band is 1.7 eV wider in h -BN than in z -BN), but the total width of the valence band is nearly as large as in graphite. The prediction of an indirect gap for h -BN agrees very well with the recent FLAPW calculations of Catellani *et al.*³⁶ and Park *et al.*³⁷ and with the OLCAO calculations of Xu and Ching.³⁸ The new results definitely settle the controversy existing in the literature (see, e.g., the brief summary given in Ref. 36).

For rhombohedral BN our calculations predict an almost unchanged width of the σ and π valence band, but a slight increase of both the direct and indirect gaps and of the internal σ - π gap relative to h -BN. Again this difference is consistent with that observed between the hexagonal and rhombohedral phases of graphite.

V. CONCLUSIONS

We have presented a general study of the structural, cohesive, and electronic properties of the tetrahedral, layered, and high-pressure phases of carbon and boron nitride. We think that our work is relevant in two respects: (i) It represents a consistent set of *ab initio* calculations of the structural and electronic properties of these very interesting and technologically important materials. To date, although both carbon and boron-nitride had been studied extensively using *ab initio* techniques, the data available in the literature have been based on different computational techniques and different potentials. Our calculations achieve full agreement with the most accurate *ab initio* calculations present so far, and should help in some case (e.g., concerning the relative energies of the tetrahedral and layered phases of BN) to settle an existing dispute. (ii) Our calculations have been performed using a carefully optimized ultrasoft (Vanderbilt-type) pseudopotential which allows us to use cutoff energies of the expansion of the wave functions which may be as low as 300 eV (i.e., of the same order of magnitude as the plane-wave cutoffs necessary for conventional norm-

TABLE VIII. Summary of the electronic band structure of BN in different crystal structures: bandwidths and minimum gaps.

	Bandwidths			Gaps	
	Lower valence band (σ) (eV)	Upper valence band (π) (eV)	Full valence band (eV)	direct (eV)	indirect
Zinc-blende					
Present work	6.2	11.0	20.4	8.8 (Γ)	4.4 (Γ - X)
Wentzov <i>et al.</i> ^a	5.9	10.8	20.3	8.6 (Γ)	4.2 (Γ - X)
Xu and Ching ^b	6.9	10.9	21.1	8.7 (Γ)	5.2 (Γ - X)
Park <i>et al.</i> ^c	5.9	10.7	20.1	8.8 (Γ)	4.4 (Γ - X)
Expt. ^{d,e}	5.2	13.5	22.0	14.5 (Γ)	(Γ - X) 6.4 (Γ - X)
Wurtzite					
Present work	6.3	11.3	20.6	8.3 (Γ)	4.9 (Γ - K)
Xu and Ching ^b	6.3	11.8	21.0	8.0 (Γ)	5.8 (Γ - K)
Park <i>et al.</i> ^c	6.0	11.0	20.3	8.2 (Γ)	4.9 (Γ - K)
Hexagonal					
Present work	4.0	9.0	17.8	4.5 (M)	4.1 (H - M)
Xu and Ching ^b	4.0	10.4	18.8	4.6 (M)	4.1 (H - M)
Park <i>et al.</i> ^c	3.8	9.0	17.7		4.0 (H - M)
Catellani <i>et al.</i> ^f	3.2	9.5	19.2	4.3 (H)	3.9 (H - M)
Expt. ^g	5.8		15-20		
Expt. ^h				3.8-5.8	
Expt. ⁱ				5.0-5.7	
Rhombohedral					
Present work	4.0	9.1	17.8	4.8 (M)	3.9 (K - M)

^aReference 33.^bReference 38, OLCAO.^cReference 37, FLAPW.^dExpt. data, as compiled in Ref. 81.^eExpt., Ref. 82.^fReference 36, FLAPW.^gExpt., Ref. 83.^hAbsorption studies, Refs. 84,85.ⁱOptical data, Refs. 86,87.

conserving pseudopotentials for simple metals and semiconductors such as Al and Si). Nevertheless, all relevant results (even structural energy differences) are shown to be well converged. This is a rather important result since it opens the way for *ab initio* studies of complex problems with many inequivalent atomic sites such as surface reconstruction, reactions at surface defects in the crystalline phases, and liquid and amorphous phases. These problems may be solved using *ab initio* molecular dynamics based on the variational solution of the Kohn-Sham equations described here, and the use of accurate ultra-

soft pseudopotentials is essential to achieve adequate convergence.

ACKNOWLEDGMENTS

This work has been supported by the Austrian Science Foundation (Fonds zur Förderung der wissenschaftlichen Forschung in Österreich) under Project No. S5908-PHYS within the framework of the trinational German-Austrian-Swiss Research Cooperation on Superhard Materials (D-A-CH).

¹ See, e.g., *SiC, Natural and Synthetic Diamond and Related Materials*, edited by A.A. Gippius, R. Hellbrig, and J.P.F. Sellschop (North-Holland, Amsterdam, 1992).

² *Synthesis and Properties of Boron Nitride*, edited by J.J. Pouch and S.A. Alterovitz (Trans-Tech, Ackermannsdorf, Switzerland, 1990).

³ J.D. Bernal, Proc. R. Soc. London Ser. A **160**, 749 (1924).

⁴ H. Lipson and A.R. Stokes, Proc. R. Soc. London A **181**, 101 (1942).

⁵ J. Donohue, *The Structures of the Elements* (Krieger, Malabar, FL, 1992).

⁶ F.D. Bundy and J.S. Kaspar, J. Chem. Phys. **46**, 3437 (1967).

⁷ M.T. Yin and M.L. Cohen, Phys. Rev. Lett. **50**, 2006

(1983).

⁸ R. Biswas, R.M. Martin, R.J. Needs, and O.H. Nielsen, Phys. Rev. B **30**, 3210 (1984).

⁹ R.S. Pearse, Acta Crystallogr. **5**, 536 (1952).

¹⁰ F.P. Bundy and R.H. Wentorf, J. Chem. Phys. **38**, 1144 (1963).

¹¹ M. Wakatsuki, K. Ichonose, and T. Aoki, Mater. Res. Bull. **7**, 999 (1972).

¹² D.R. McKenzie *et al.*, J. Non-Cryst. Solids **164-166**, 1101 (1993).

¹³ See, e.g., the articles by Y. Catherine *et al.*, in *Diamond and Diamond-like Carbon*, edited by R. Clausing *et al.* (Plenum, New York, 1991).

¹⁴ Y. Osaka, A. Chayahara, H. Yokoyama, M. Okamoto, T.

- Hamado, and M. Fujisawa, in *Synthesis and Properties of Boron Nitride* (Ref. 2), p. 227.
- ¹⁵ P.C. Kelires, C.H. Lee, and W.R. Lambrecht, *J. Non-Cryst. Solids* **164-166**, 1131 (1993).
 - ¹⁶ P.M. Gaskell, A. Saeed, P. Chieux, and D.R. McKenzie, *J. Non-Cryst. Solids* **150**, 126 (1992).
 - ¹⁷ P. Hohenberg and W. Kohn, *Phys. Rev.* **136**, B864 (1964); W. Kohn and L.J. Sham, *ibid.* **140**, A1133 (1965).
 - ¹⁸ W.E. Pickett, *Comput. Phys. Rep.* **9**, 115 (1989).
 - ¹⁹ S. Ihm, *Rep. Prog. Phys.* **51**, 105 (1988).
 - ²⁰ R. Car and M. Parrinello, *Phys. Rev. Lett.* **55**, 2471 (1985).
 - ²¹ M.P. Teter, M.C. Payne, and D.C. Allan, *Phys. Rev. B* **40**, 12255 (1989); M.C. Payne, M.P. Teter, D.C. Allan, T.A. Arias, and J.D. Joannopoulos, *Rev. Mod. Phys.* **64**, 1045 (1992).
 - ²² G. Kresse and J. Hafner, *Phys. Rev. B* **47**, 588 (1993).
 - ²³ M.T. Yin, *Phys. Rev. B* **30**, 1773 (1984).
 - ²⁴ M.T. Yin and M.L. Cohen, *Phys. Rev. B* **29**, 6996 (1984).
 - ²⁵ R. Biswas, R.M. Martin, R.J. Needs, and O.H. Nielsen, *Phys. Rev. B* **35**, 9599 (1987).
 - ²⁶ J.C. Charlier, X. Gonze, and J.P. Michenaud, *Phys. Rev. B* **43**, 4579 (1991).
 - ²⁷ S. Fahy, S.G. Louie, and M.L. Cohen, *Phys. Rev. B* **34**, 1191 (1986).
 - ²⁸ S. Fahy and S.G. Louie, *Phys. Rev. B* **36**, 3373 (1987).
 - ²⁹ A.K. McMahan, *Phys. Rev. B* **30**, 5835 (1984).
 - ³⁰ H.J.F. Jansen and A.J. Freeman, *Phys. Rev. B* **35**, 8207 (1987).
 - ³¹ J.L. Warren, J.L. Yarnell, G. Dolling, and R.A. Cowley, *Phys. Rev.* **158**, 805 (1967).
 - ³² R.M. Niklow, N. Wakabayashi, and H.G. Smith, *Phys. Rev. B* **5**, 4951 (1972).
 - ³³ R.M. Wentzcovitch, K.J. Chang, and M.L. Cohen, *Phys. Rev. B* **34**, 1071 (1986).
 - ³⁴ R.M. Wentzcovitch, M.L. Cohen, and P.K. Lam, *Phys. Rev. B* **36**, 6058 (1987).
 - ³⁵ R.M. Wentzcovitch, S. Fahy, M.L. Cohen, and S.G. Louie, *Phys. Rev. B* **38**, 6191 (1988).
 - ³⁶ A. Catellani, M. Pasternak, A. Baldereschi, and A.J. Freeman, *Phys. Rev. B* **36**, 6105 (1987).
 - ³⁷ K.T. Park, K. Terakura, and N. Hamada, *J. Phys. C* **20**, 1241 (1987).
 - ³⁸ Y.N. Xu and W.Y. Ching, *Phys. Rev. B* **44**, 7787 (1991).
 - ³⁹ G. Kerker, *J. Phys. C* **13**, L189 (1980).
 - ⁴⁰ D.R. Hamann, M. Schlüter, and C. Chang, *Phys. Rev. Lett.* **43**, 1494 (1979).
 - ⁴¹ D. Vanderbilt, *Phys. Rev. B* **32**, 8412 (1985).
 - ⁴² G.B. Bachelet, D.R. Hamann, and M. Schlüter, *Phys. Rev. B* **26**, 4199 (1982).
 - ⁴³ A.M. Rappe, K.M. Rabe, E. Kaxiras, and J.D. Joannopoulos, *Phys. Rev. B* **41**, 1227 (1990).
 - ⁴⁴ N. Troullier and J.L. Martins, *Phys. Rev. B* **48**, 1993 (1991).
 - ⁴⁵ G. Kresse, J. Hafner, and R.J. Needs, *J. Phys. Condens. Matter* **4**, 7451 (1992).
 - ⁴⁶ J.L. Lin, A. Qteish, M.C. Payne, and V. Heine, *Phys. Rev. B* **47**, 4174 (1993).
 - ⁴⁷ G. Kresse and J. Hafner, *J. Phys. Condens. Matter* (to be published).
 - ⁴⁸ D. Vanderbilt, *Phys. Rev. B* **41**, 7892 (1990).
 - ⁴⁹ K. Laasonen, R. Car, C. Lee, and D. Vanderbilt, *Phys. Rev. B* **43**, 6796 (1991); K. Laasonen, A. Pasquarello, R. Car, C. Lee, and D. Vanderbilt, *ibid.* **47**, 10142 (1993).
 - ⁵⁰ G. Kresse and J. Hafner, *Phys. Rev. B* **48**, 13115 (1993).
 - ⁵¹ G. Kresse and J. Hafner, *Phys. Rev. B* **49**, 14251 (1994).
 - ⁵² D.M. Bylander and L. Kleinman, *Phys. Rev. B* **46**, 13756 (1992).
 - ⁵³ R.D. King-Smith, M.C. Payne, and J.S. Lin, *Phys. Rev. B* **44**, 13063 (1991).
 - ⁵⁴ G. Kresse, Ph.D. thesis, Technische Universität Wien, 1993.
 - ⁵⁵ C.G. Broyden, *Math. Comput.* **19**, 577 (1965).
 - ⁵⁶ H.J. Monkhorst and J.D. Pack, *Phys. Rev. B* **13**, 5188 (1976); D.J. Chadi and H.L. Cohen, *ibid.* **8**, 5747 (1973).
 - ⁵⁷ N.D. Mermin, *Phys. Rev.* **137**, A1141 (1965).
 - ⁵⁸ M. Weinert and J.W. Davenport, *Phys. Rev. B* **45**, 13709 (1992); R.M. Wentzcovitch, J.L. Martins, and P.B. Allen, *ibid.* **45**, 11372 (1992).
 - ⁵⁹ A. de Vita and M.J. Gillan, *J. Phys. Condens. Matter* **3**, 6225 (1991).
 - ⁶⁰ D.D. Johnson, *Phys. Rev. B* **38**, 12807 (1988).
 - ⁶¹ P. Pulay, *Mol. Phys.* **17**, 197 (1969).
 - ⁶² S. Goldecker and K. Maschke, *Phys. Rev. B* **45**, 1597 (1992).
 - ⁶³ F.D. Murnaghan, *Proc. Natl. Acad. Sci. USA* **30**, 244 (1944).
 - ⁶⁴ J. Furthmüller and J. Hafner (unpublished).
 - ⁶⁵ L. Brewer (unpublished, as cited in Refs. 28 and 24).
 - ⁶⁶ H.J. McSkimin, P. Andreatch, and P. Glynn, *J. Appl. Phys.* **43**, 985 (1972).
 - ⁶⁷ K. Gschneidner, *Solid State Phys.* **16**, 275 (1964).
 - ⁶⁸ R.E. Hanneman, H.M. Strong, and F.B. Bundy, *Science* **155**, 995 (1967).
 - ⁶⁹ C. Frondel and U.B. Marvin, *Nature* **214**, 587 (1967).
 - ⁷⁰ E. Wigner, *Phys. Rev.* **46**, 1002 (1934).
 - ⁷¹ We use the parametrization presented by J.P. Perdew and A. Zunger, *Phys. Rev. B* **23**, 5048 (1981).
 - ⁷² H.A. Jishi and G. Dresselhaus, *Phys. Rev. B* **26**, 4514 (1982).
 - ⁷³ W. Weber, *Phys. Rev. B* **15**, 4789 (1977).
 - ⁷⁴ M. Kertesz and R. Hoffmann, *Solid State Commun.* **54**, 313 (1984).
 - ⁷⁵ S. Fahy, K.J. Chang, S.G. Louie, and M.L. Cohen, *Phys. Rev. B* **35**, 5856 (1987).
 - ⁷⁶ C.D. Clark, P.J. Dean, and P.V. Harris, *Proc. R. Soc. London A* **277**, 312 (1964).
 - ⁷⁷ M.C. Schabel and J.L. Martins, *Phys. Rev. B* **46**, 7185 (1992).
 - ⁷⁸ N.A.W. Holzwarth, S.G. Louie, and S. Rabii, *Phys. Rev. B* **26**, 5382 (1982).
 - ⁷⁹ W. Eberhardt, J.T. McGovern, E.W. Plummer, and J.E. Fischer, *Phys. Rev. Lett.* **44**, 200 (1980).
 - ⁸⁰ A.R. Law, J.J. Barry, and H.P. Hughes, *Phys. Rev. B* **28**, 5332 (1983).
 - ⁸¹ *Physics of Group IV Elements and III-IV Compounds*, edited by O. Madelung, Landolt-Börnstein, New Series, Group III, Vol. 17a (Berlin, Springer, 1982).
 - ⁸² V.A. Fomichev and M.A. Punsh, *J. Chem. Phys.* **48**, 555 (1968).
 - ⁸³ E. Zegeler, N. Kosuch, G. Wiech, and A. Faessler, *Phys. Status Solidi B* **91**, 223 (1979).
 - ⁸⁴ A. Zunger, A. Katzir, and A. Halperin, *Phys. Rev. B* **13**, 5560 (1976).
 - ⁸⁵ M.J. Rand and J.F. Roberts, *J. Electrochem. Soc.* **115**, 422 (1968).
 - ⁸⁶ V. Büchner, *Phys. Status Solidi B* **81**, 227 (1977).
 - ⁸⁷ R.D. Leapman, P.L. Fejes, and J. Silcox, *Phys. Rev. B* **28**, 2351 (1983).